847
Journal of Organometallic Chemistry xxx (2017) xxx–xxx 204-212.

Contents lists available at ScienceDirect

Journal of Organometallic Chemistry

journal homepage: www.elsevier.com/locate/jorganchem

Synthesis, structural characterization, and volatility evaluation of zirconium and hafnium amidate complexes

Mahesh C. Karunarathne, Joseph W. Baumann, Mary Jane Heeg, Philip D. Martin, Charles H. Winter*

Department of Chemistry, Wayne State University, Detroit, MI 48202, USA

ARTICLE INFO

Article history:
Received 9 February 2017
Received in revised form
1 March 2017
Accepted 2 March 2017
Available online xxx
Published 01 Oct. 2017

Keywords:
Zirconium
Hafnium
Amidate ligand
Precursor
Atomic layer deposition
Chemical vapor deposition

ABSTRACT

Treatment of tetrakis(dimethylamido)zirconium or tetrakis(dimethylamido)hafnium with four equivalents of N-*tert*-butylacetamide, N-isopropylisobutyramide, N-isopropylacetamide, N-methylacetamide, or N-*tert*-butylformamide in refluxing toluene, followed by sublimation of the crude products at 105–125 °C/0.05 Torr, afforded tetrakis(N-*tert*-butylacetamido)zirconium (81%), tetrakis(N-isopropylisobutyramido)zirconium (87%), tetrakis(N-isopropylacetamido)zirconium (51%), tetrakis(N-*tert*-butylacetamido)hafnium (83%), tetrakis(N-isopropyliso-butyramido)hafnium (79%), tetrakis(N-isopropylacetamido)hafnium (67%), tetrakis(N-methylacetamido)zirconium (5%), and tetrakis(N-*tert*-butylformamido)zirconium (1%) as colorless crystalline solids. The structural assignments for the new complexes were based upon spectral and analytical data and by X-ray crystal structure determinations for tetrakis(N-*tert*-butylacetamido)zirconium, tetrakis(N-isopropylacetamido)zirconium, tetrakis(N-isopropylacetamido)hafnium, tetrakis(N-methylacetamido)zirconium, and tetrakis(N-*tert*-butylformamido)zirconium. These complexes are monomeric in the solid state, with eight-coordinate metal centers surrounded by four κ^2-N,O-amidate ligands. Six of the eight new complexes undergo sublimation on a preparative scale from 130 to 140 °C at 0.05 Torr, with 84.5–95.8% sublimed recoveries and 0.68–3.06% nonvolatile residues. Tetrakis(N-methylacetamido)zirconium and tetrakis(N-*tert*-butylformamido)zirconium decompose extensively upon attempted sublimation. Solid state decomposition temperatures for the zirconium complexes range between 218 and 335 °C and 290–360 °C for the hafnium complexes. Tetrakis(N-isopropylisobutyramido)zirconium, tetrakis(N-*tert*-butylacetamido)hafnium, and tetrakis(N-isopropylacetamido)hafnium exhibit the highest solid state decomposition temperatures in the series, possess good volatility, and have useful properties for chemical vapor deposition and atomic layer deposition precursors.

1. Introduction

HfO_2 is widely used as the gate dielectric material in metal oxide semiconductor field-effect transistors [1,2]. Moreover, ternary and quaternary HfO_2-based materials are of significant interest as advanced high-κ material substitutes in future microelectronics devices [3–10]. ZrO_2 [10–15] and other zirconium-containing high-κ materials [16–20] are also structurally compatible with silicon semiconductors and are of interest as alternative gate dielectrics in future transistor structures. Zirconium- and hafnium-based thin films are also components in capacitors [4–7,21], tunnel junctions [22–24], and optical coatings [25–27], due to their high dielectric constants, low leakage currents, interface compatibility with Si and SiO_2, high chemical and thermodynamic stability in contact with Si at elevated temperatures, large band gap energies, and high refractive indices.

Atomic layer deposition (ALD) [28–30] has been widely used to grow ZrO_2 and HfO_2 films, for several reasons. The self-limited growth mechanism of ALD gives constant growth rates per cycle, which allows sub-nanometer control over film thicknesses [28–30]. The dielectric layers used in transistor structures need to be <10 nm thick, and the thicknesses and uniformities must be precisely controlled. The surfaces must also be atomically smooth to avoid the accumulation of trapped interface charges [1a]. Moreover, the self-limited ALD growth mechanism enables high conformal coverage in nanoscale features, since growth occurs in a

* Corresponding author.
E-mail address: chw@chem.wayne.edu (C.H. Winter).

http://dx.doi.org/10.1016/j.jorganchem.2017.03.003
0022-328X/

layer-by-layer fashion [28–30]. Applications such as resistive random access memories and vertical transistor designs require perfect growth of conformal dielectric coatings in high aspect features as well as excellent film thickness control [24,31]. ALD precursors must combine volatility, thermal stability at the film growth temperature, and high reactivity toward a second reagent to afford the desired thin film material [28–30]. The tetragonal and cubic phases of ZrO_2 and HfO_2 have higher κ values than the monoclinic phase or amorphous films, and growth of the tetragonal and cubic phases is favored at deposition temperatures of >300 °C [32–34]. Additionally, growth at >300 °C affords higher density films with better crystallinity, compared to films grown at lower temperatures. Precursors containing many different ligands have been used in the ALD growth of ZrO_2 and HfO_2 films [32–34], of which selected examples include halides [35,36], dialkylamides [37–39], alkoxides [40–42], cyclopentadienyls [32–34,43–47], and others [48–51]. Zirconium and hafnium halides have high thermal stabilities and high growth rates, but form corrosive HX as a reaction byproduct, lead to undesired halogen impurities in the films, and are powders that can lead to particle incorporation into the films [32–36]. Dialkylamides have good volatility, high reactivity, and high growth rates, but carbon and nitrogen incorporation in the films can be a problem and their low thermal stabilities limit deposition temperatures to <300 °C [32–34,37–39]. Cyclopentadienyl-based precursors can have high thermal stabilities, but growth rates are often lower than those of halides and dialkylamides and the reactivities are not as high as those of dialkylamides [32–34,43–47]. For these reasons, there is continuing interest in the development of new precursors for ZrO_2 and HfO_2 films that combine volatility, high thermal stability, high reactivity toward oxygen sources, and high growth rates in ALD processes.

In contemplating new directions for zirconium and hafnium ALD precursors, we sought to identify ligands that would confer high thermal stabilities. Organic amides have strong C-N and C-O bonds due to delocalization, and are widely used in organic polymers that exhibit high thermal stabilities [52]. Amidate ligands derived from deprotonation of organic amides containing N-H bonds therefore might lead to new classes of highly thermally stable precursors. Zirconium and hafnium complexes containing amidate ligands have been reported recently, mostly within the context of catalyst development for organic transformations [53–64]. Most of these zirconium and hafnium complexes contain mixed ligand sets with amidates and other ligands. Only a few complexes of the formula M(amidate)$_4$ (M = Zr, Hf) have been reported [51,53,64]. Herein we describe the synthesis, structure, properties, volatility, and thermal stability of zirconium and hafnium amidate complexes of the formula M(RC(O)NR′)$_4$ (M = Zr(IV), Hf(IV)). Many of these new complexes sublime at moderate temperatures under reduced pressures and have decomposition temperatures above 300 °C. These properties suggest that the new amidate complexes may serve as useful ALD and chemical vapor deposition (CVD) precursors.

2. Results and discussion

2.1. Synthesis of new complexes

Treatment of tetrakis(dimethylamido)zirconium with four equivalents of N-*tert*-butylacetamide, N-isopropylisobutyramide, or N-isopropylacetamide in refluxing toluene, followed by sublimation of the crude products at 110–120 °C/0.05 Torr, afforded tetrakis(N-*tert*-butylacetamido)zirconium (**1**, 81%), tetrakis(N-isopropylisobutyr-amido)zirconium (**2**, 87%), and tetrakis(N-isopropylacetamido)zirconium (**3**, 51%), respectively, as colorless crystalline solids (eq 1). Similar treatment of tetrakis(dimethylamido)hafnium with the same amides afforded tetrakis(N-*tert*-butylacetamido)hafnium (**4**, 83%), tetrakis(N-isopropylisobutyramido)hafnium (**5**, 79%), and tetrakis(N-isopropylacetamido)hafnium (**6**, 67%), as colorless crystalline solids (eq 1). The synthesis of lower molecular weight complexes was explored by treatment of tetrakis(dimethylamido)zirconium with N-methylacetamide and N-*tert*-butylformamide in refluxing toluene, to afford tetrakis(N-methylacetamido)zirconium (**7**) and tetrakis(N-*tert*-butylformamido)zirconium (**8**), respectively (eq 1). Sublimation of the crude product mixtures afforded very low yields of **7** (~5%) and **8** (~1%), although the products were obtained as high purity single crystals. The syntheses were repeated, but **7** and **8** were extracted with hexane from the crude reaction residues obtained upon removal of the toluene. Filtration through a pad of Celite, followed by removal of the hexane under reduced pressure, afforded the products with ~95% purity by ^{1}H NMR and in much higher yields (**7**, 77%; **8**, 47%). Accordingly, **7** and **8** appear to decompose substantially upon sublimation. The lower thermal stabilities of **7** and **8**, compared to **1**–**6**, may arise because of the smaller amidate carbon and nitrogen atom substituents, which allow more access to the polar, reactive zirconium-oxygen and zirconium-nitrogen bonds. Additional experiments were conducted in which tetrakis(dimethylamido)zirconium was treated in refluxing toluene with four equivalents of the primary organic amides acetamide, isobutyramide, and trimethylacetamide or the secondary organic amide N-isopropylformamide. Analysis of the crude products by ^{1}H NMR showed complex mixtures, and these reactions were not pursued further.

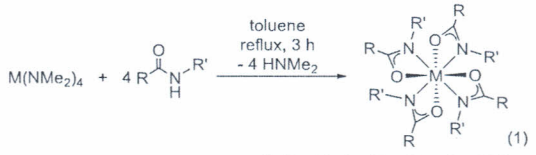

(1)

1, M = Zr, R = Me, R′ = tBu, 81%
2, M = Zr, R = iPr, R′ = iPr, 87%
3, M = Zr, R = Me, R′ = iPr, 51%
4, M = Hf, R = Me, R′ = tBu, 83%
5, M = Hf, R = iPr, R′ = iPr, 79%
6, M = Hf, R = Me, R′ = iPr, 67%
7, M = Zr, R = Me, R′ = Me, 5%
8, M = Zr, R = H, R′ = tBu, 1%

The structural assignments for **1**–**8** were based upon spectral and analytical data and by X-ray crystal structure determinations for **1**, **3**, **6**, **7**, and **8**, as described below. Due to poor quality crystals, structure determinations for **2** and **5** were not possible. A low precision X-ray crystal structure determination of **4** revealed a molecular structure similar to that of **1**. Complexes **1**, **3**, **4**, **6**, **7**, and **8** are monomeric in the solid state, with eight-coordinate metal centers surrounded by four κ^2-N,O-amidate ligands. Complexes **2** and **5** likely possess similar molecular structures. The ^{1}H and ^{13}C {^{1}H} NMR spectra of **1**–**8** in benzene-d_6 are consistent with the solid state structure assignments and show only one set of resonances for all four amidate ligands in the same chemical environment. Complexes **1** and **2** were reported recently [64]. The NMR spectra for **1** and **2** described herein are identical to the previously reported values. In the present study, melting points were observed for **1** (255–258 °C) and **2** (285–288 °C), whereas the previous paper [64] stated that the complexes did not melt up to their decomposition temperatures.

2.2. X-ray structural aspects

The X-ray crystal structures of **1**, **3**, **6**, **7**, and **8** were determined to establish the geometries about the metal centers and the

Please cite this article in press as: M.C. Karunarathne, et al., Journal of Organometallic Chemistry (2017), http://dx.doi.org/10.1016/j.jorganchem.2017.03.003

amidate ligand bonding modes. Crystallographic data are summarized in Table 1 and selected bond lengths and angles are given in Tables 2 and 3. Figs. 1–5 show the perspective views of **1**, **3**, **6**, **7**, and **8**.

Complexes **1**, **3**, **6**, and **7**, and **8** exist as eight-coordinate monomers in which the amidate ligands are coordinated in a chelating κ^2-N,O-fashion through the amidate nitrogen and oxygen atoms. The geometry around the zirconium and hafnium metal centers can be approximated as dodecahedral. In **1**, **3**, **6**, and **8**, four amidate ligand nitrogen atoms form an approximate square plane around the metal center and four oxygen donor atoms occupy apical positions, with one pair above and one pair below the four nitrogen atom square plane. The geometry in **7** is also dodecahedral, except that the approximate square plane is composed of three nitrogen atoms and one oxygen atom, and the apical pairs consist of two oxygen atoms and one nitrogen and one oxygen atom. The slightly different ligand arrangement in **7** may occur because the amidate nitrogen atoms have the least sterically demanding substituents (methyl groups). The metal-oxygen bond lengths associated with the amidate ligands (**1**, 2.173(1)-2.185(1) Å; **3**, 2.197(1)-2.222(1) Å; **6**, 2.183(4)-2.206(4) Å, **7**, 2.201(1)-2.234(1) Å; **8**, 2.194(3)-2.219(3) Å) are very similar and show no trend with the steric bulk of the amidate ligand substituents. The metal-nitrogen bond lengths (**1**, 2.310(1)-2.328(2) Å; **3**, 2.270(1)-2.297(1) Å; **6**, 2.248(5)-2.284(5) Å; **7**, 2.237(1)-2.266(1) Å; **8**, 2.276(3)-2.300(3) Å) are similar for **1**, **3**, and **8**, but are slightly shorter for the hafnium complex **6**. The ionic radius of hafnium(IV) (r = 0.71 Å for six coordination) is slightly smaller than that of zirconium(IV) (r = 0.72 Å for six coordination) [65], which accounts for the slightly shorter metal-nitrogen bond distances in **6**, compared to **3**. The slightly shorter zirconium-nitrogen distances in **7**, compared to **1**, **3**, and **8**, may arise from the small steric profile of the methyl groups on the amidate core nitrogen atoms. The nitrogen square planes in **1**, **3**, **6**, and **8** are characterized by angles close to 90° (**1**, 88.95(4)-92.50(5)°; **3**, 88.01(5)-93.26(5)°; **6**, 88.85(19)-92.7(2)°; **8**, 88.61(12)-92.27(12)°). In **7**, the N_3O square plane has angles that range from 82.21(5)-92.95(5)°. There are two different types of oxygen-metal-oxygen angles in **1**, **3**, **6**, and **8**, one in which the two oxygen atoms are located on the same side of the plane of nitrogen atoms (**1**, 75.12(3), 75.78(3)°; **3**, 74.08(4), 74.88(4)°; **6**, 73.90(15), 74.67(16)°; **8**, 75.44(10), 76.00(10)°) and one in which they are on the opposite side of the plane (**1**, 127.44(4)-130.33(4)°; **3**, 127.07(4)-131.29(4)°; **6**, 127.41(16)-131.19(16)°; **8**, 126.38(10)-131.14(11)°). The nitrogen-metal-oxygen bite angles within each amidate ligand are also similar and range from 58.14(5) to 59.44(19)°. Relevant structurally characterized zirconium and hafnium amidate complexes are limited to $Hf(iPrOC(O)NiPr)_4$ [51], $Hf(MeEtNC(O)NiPr)_4$ [51], $Zr(tBuC(O)N(2,6\text{-}Me_2\text{-}C_6H_4))_4$ [53], $Hf(PhC(O)N(2,6\text{-}Me_2\text{-}C_6H_4))_4$ [53], $Zr(iPrC(O)NtBu)_4$ [64], $Zr(tBuC(O)NiPr)_4$ [64], and $Zr(iPrC(O)NiPr)_4$ [64]. All of these complexes are mononuclear and exhibit approximate dodecahedral geometry. The metal-oxygen and metal-nitrogen bond lengths in $Hf(iPrOC(O)NiPr)_4$ (Hf-O 2.208–2.238 Å; Hf-N 2.231–2.252 Å),

Table 2
Selected Bond lengths (Å) and Angles (deg) for **1**, **3**, **6**, and **7**.

	1 (M = Zr)	**3** (M = Zr)	**6** (M = Hf)	**7** (M = Zr)
M-O(1)	2.183(1)	2.207(1)	2.198(4)	2.211(1)
M-O(2)	2.185(1)	2.197(1)	2.183(4)	2.234(1)
M-O(3)	2.173(1)	2.222(1)	2.206(4)	2.201(1)
M-O(4)	2.183(1)	2.203(1)	2.201(4)	2.227(1)
M(1)-N(1)	2.328(2)	2.297(1)	2.284(5)	2.252(1)
M(1)-N(2)	2.310(1)	2.272(1)	2.248(5)	2.237(1)
M(1)-N(3)	2.316(1)	2.290(1)	2.273(5)	2.237(1)
M(1)-N(4)	2.323(2)	2.270(1)	2.253(5)	2.266(1)
O(1)-M-O(2)	127.45(4)	127.78(4)	128.43(15)	80.15(4)
O(1)-M-O(3)	129.74(4)	74.88(4)	74.67(16)	84.23(4)
O(1)-M-O(4)	75.12(3)	131.27(4)	130.82(15)	124.38(4)
O(2)-M-O(3)	75.78(3)	131.29(4)	131.19(16)	81.91(4)
O(2)-M-O(4)	130.33(4)	74.08(4)	73.90(15)	127.95(4)
O(3)-M-O(4)	127.44(4)	127.07(4)	127.41(16)	138.62(4)
N(1)-M-N(2)	88.95(4)	91.10(5)	90.5(2)	92.95(5)
N(1)-M-N(3)	92.26(5)	168.71(4)	168.1(2)	162.74(4)
N(1)-M-N(4)	168.17(4)	88.01(5)	88.85(19)	82.21(5)
N(2)-M-N(3)	167.51(4)	89.79(5)	90.28(19)	90.43(6)
N(2)-M-N(4)	88.74(5)	168.86(5)	168.26(19)	138.56(5)
N(3)-M-N(4)	92.50(5)	93.26(5)	92.7(2)	84.07(5)
O(1)-M-N(1)	58.14(5)	58.25(4)	58.67(19)	58.77(4)
O(2)-M-N(2)	58.25(3)	58.68(4)	59.44(19)	58.60(4)[a]
O(3)-M-N(3)	58.46(3)	58.16(4)	58.53(17)	58.75(5)[a]
O(4)-M-N(4)	58.18(5)	58.59(4)	58.57(16)	58.66(5)[a]

[a] Due to different atom numbering in **7**, these angles correspond to O(2)-Zr-N(3), (O3)-Zr-N(4), and O(4)-Zr-N(2), respectively.

Table 3
Selected Bond lengths (Å) and Angles (deg) for **8**.

Zr(02)-O(004)	2.199(3)	Zr(02)-N(009)	2.276(3)
Zr(02)-O(005)	2.194(3)	Zr(02)-N(00B)	2.300(3)
Zr(02)-O(006)	2.213(3)	Zr(02)-N(00C)	2.285(3)
Zr(02)-O(008)	2.219(3)	Zr(02)-N(00D)	2.290(3)
O(004)-Zr(02)-O(005)	75.44(10)	N(009)-Zr(02)-N(00b)	91.11(11)
O(004)-Zr(02)-O(006)	129.93(11)	N(009)-Zr(02)-N(00c)	91.03(12)
O(004)-Zr(02)-O(008)	126.38(10)	N(009)-Zr(02)-N(00d)	166.59(11)
O(005)-Zr(02)-O(006)	126.88(10)	N(00b)-Zr(02)-N(00c)	166.90(12)
O(005)-Zr(02)-O(008)	131.14(11)	N(00b)-Zr(02)-N(00d)	88.61(12)
O(006)-Zr(02)-O(008)	76.00(11)	N(00c)-Zr(02)-N(00d)	92.27(12)
O(004)-Zr(O2)-N(00d)	58.70(10)	O(005)-Zr(O2)-N(009)	59.22(10)
O(006)-Zr(O2)-N(00b)	58.67(11)	O(008)-Zr(O2)-N(00c)	58.48(11)

Table 1
Crystal data and data collection parameters for **1**, **3**, and **6**–**8**.

	1	**3**	**6**	**7**	**8**
Formula	$C_{24}H_{48}N_4OZr$	$C_{20}H_{40}N_4O_4Zr$	$C_{20}H_{40}HfN_4O_4$	$C_{12}H_{24}N_4O_4Zr$	$C_{15}H_{27}N_3O_3Zr_{0.75}$
FW	547.88	491.78	579.05	379.57	365.81
space group	$Pna2_1$	I-4	I-4	$P2_1/c$	C2/c
a (Å)	11.7562(3)	22.3810(4)	22.4048(4)	11.3585(6)	21.5363(12)
b (Å)	14.7522(4)	22.3810(4)	22.4048(4)	12.3292(6)	11.6298(6)
a (Å)	16.7681(5)	10.1522(2)	10.1105(2)	11.5666(6)	31.6186(15)
V(Å^3)	2910.31(14)	5085.33(16)	5075.22(16)	1619.17(14)	7773.9(7)
Z	4	8	8	4	16
Temp (K)	100(2)	100(2)	100(2)	100(2)	100(2)
ρ_{calcd} (g cm^{-3})	1.250	1.285	1.516	1.557	1.250
μ (mm^{-1})	0.410	0.461	4.140	0.699	0.452
R(F) (%)	2.67	2.00	2.80	2.68	6.73
Rw(F) (%)	5.89	4.84	5.25	3.54	8.32

$R(F) = \sum||Fo|-|Fc|| / \sum|| Fo||$; $Rw(F) = [\sum w(Fo^2 - Fc^2)^2/\sum w(Fo^2)^2]^{1/2}$ for $I > 2\sigma(I)$.

Please cite this article in press as: M.C. Karunarathne, et al., Journal of Organometallic Chemistry (2017), http://dx.doi.org/10.1016/j.jorganchem.2017.03.003

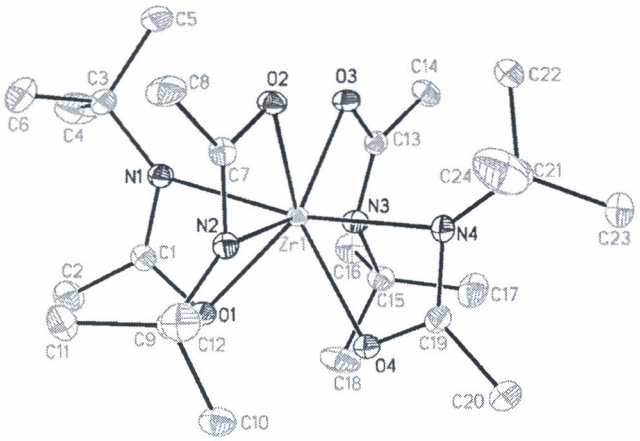

Fig. 1. Perspective view of **1** with thermal ellipsoids at the 50% probability level.

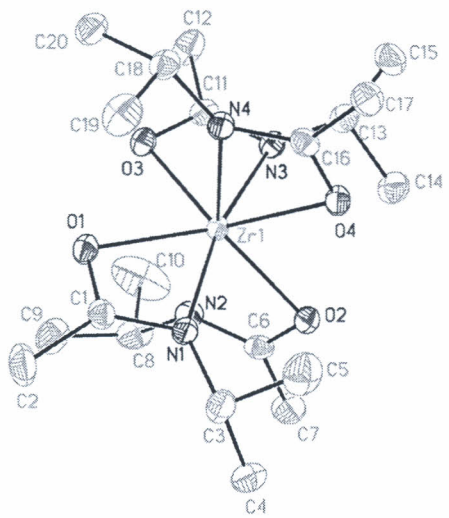

Fig. 2. Perspective view of **3** with thermal ellipsoids at the 50% probability level.

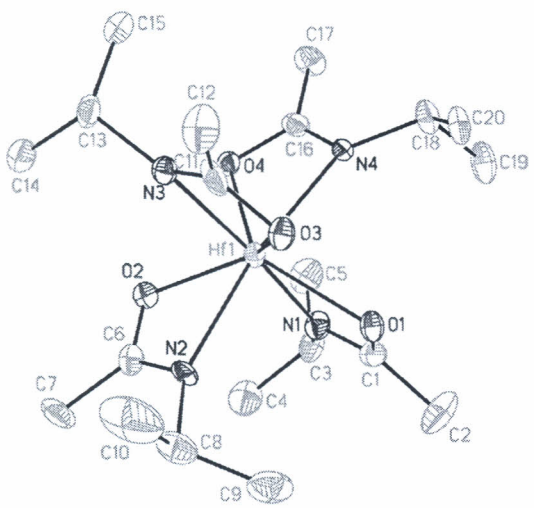

Fig. 3. Perspective view of **6** with thermal ellipsoids at the 50% probability level.

Hf(MeEtNC(O)NiPr)$_4$ (Hf-O 2.167–2.199 Å; Hf-N 2.263–2.293 Å), Zr(tBuC(O)N(2,6-Me$_2$-C$_6$H$_4$))$_4$ (Zr-O 2.114–2.124 Å; Zr-N 2.288–2.323 Å), and Hf(PhC(O)N(2,6-Me$_2$-C$_6$H$_4$))$_4$ (Hf-O 2.163 Å; Hf-N 2.325 Å), Zr(iPrC(O)NtBu)$_4$ (Zr-O 2.089–2.280 Å; Zr-N 2.298–2.378 Å), Zr(tBuC(O)NiPr)$_4$ (Zr-O 2.194–2.202 Å; Zr-N 2.289–2.315 Å), and Zr(iPrC(O)NiPr)$_4$ (Zr-O 2.189–2.207 Å; Zr-N 2.272–2.302 Å) are similar to slightly shorter than those found in **1**, **3**, **6**, **7**, and **8**. The slightly shorter bond lengths in some of these literature complexes may reflect larger steric profiles of the amidate core carbon and nitrogen substituents in **1**, **3**, **6**, **7**, and **8**. Interestingly, Hf(iPrOC(O)NiPr)$_4$ [51], Hf(MeEtNC(O)NiPr)$_4$ [51], Zr(iPrC(O)NtBu)$_4$ [64], Zr(tBuC(O)NiPr)$_4$ [64], and Zr(iPrC(O)NiPr)$_4$ adopt ligand arrangements similar to **1**, **3**, **6**, and **8**, where the amidate core ligand nitrogen atoms form an approximate square plane with the amidate core oxygen atoms in the apical positions. By contrast, Zr(tBuC(O)N(2,6-Me$_2$-C$_6$H$_4$))$_4$ [53] and Hf(PhC(O)N(2,6-Me$_2$-C$_6$H$_4$))$_4$ [53] adopt ligand arrangements in which the amidate oxygen atoms form a square plane and the amidate nitrogen atoms lie in the apical positions. The exact ligand arrangements about the metal atoms is likely subtly dependent upon the steric profiles of the amidate ligand substituents.

2.3. Volatility and thermal stability study

The volatility and thermal stability of **1**–**8** were studied to assess their viability as ALD and CVD precursors. Since **7** and **8** decomposed extensively upon sublimation, their properties were not studied in as much detail as the others. Fig. 6 shows the thermogravimetric analyses of selected compounds **2** and **3**. These compounds were chosen because they sublime with high yields and low non-volatile residues. Complexes **2** and **3** show very similar behavior, with weight loss onsets of ~175 °C and residues at 500 °C of 2.5 and 3.4%, respectively. Accordingly, **2** and **3** sublime in single step events, have low nonvolatile residues, and thus exhibit ideal behavior for application as film growth precursors. Interestingly, the thermogravimetric analysis of **2** in a previous report [64] showed a multistep weight loss process, with an onset of decomposition starting at about 150 °C and 25–30% nonvolatile residue upon reaching 400 °C. Such behavior for **2** is very different from that observed herein. It is possible that **2** was exposed to air briefly during the previous thermogravimetric analysis experiment [64], which would lead to partial decomposition. In the present work, the thermogravimetric analyses were carried out with an instrument enclosed in a glove box containing high purity nitrogen. The vapor pressures of **2** and **3** were measured using the Knudsen effusion method. Complex **2** exhibited a vapor pressure of 0.67 Torr at 190 °C, whereas the vapor pressure for **3** was 1.0 Torr at 170 °C. Accordingly, **3** is slightly more volatile than **2**, consistent with its slightly lower molecular weight and the thermogravimetric analysis trace in Fig. 6.

Preparative sublimation and decomposition temperature data for **1**–**8** are summarized in Table 4. Complexes **1**–**8** are all high melting solids, with **7** having the lowest melting point (181 °C). The capillaries were inspected under a microscope at the end of the melting point experiments, and none of the samples showed any discoloration or evidence of decomposition upon melting. To determine the solid state decomposition temperatures, a few milligrams of each complex were sealed in high purity argon-filled capillary tubes. The tubes were then heated at a rate of 5 °C/min starting at 25 °C until there was qualitative evidence of decomposition through discoloration of the initially colorless samples. Complexes **1**–**8** all undergo abrupt visual discoloration from colorless to orange-brown liquids, and have decomposition temperatures of 280, 335, 270, 300, 360, 290, 218, and 263 °C, respectively. These thermal decomposition temperatures were

Please cite this article in press as: M.C. Karunarathne, et al., Journal of Organometallic Chemistry (2017), http://dx.doi.org/10.1016/j.jorganchem.2017.03.003

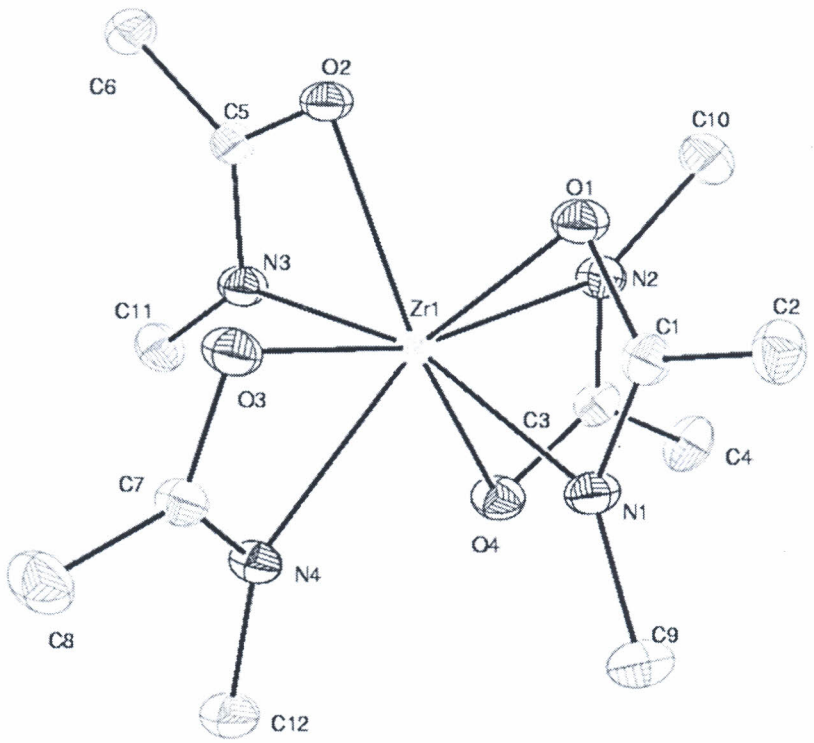

Fig. 4. Perspective view of **7** with thermal ellipsoids at the 50% probability level.

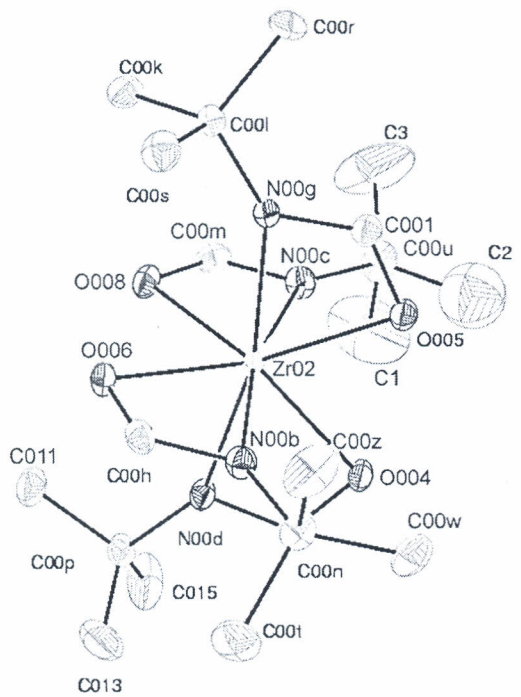

Fig. 5. Perspective view of **8** with thermal ellipsoids at the 50% probability level.

established unambiguously by heating two sets of samples in sealed melting point tubes to 5 °C below their visual decomposition temperatures, and then remelting the first set of samples and by taking ^{1}H NMR spectra of the other set of samples. For **1**–**6**, the melting points of the first set of samples were identical to those of virgin samples, and the ^{1}H NMR spectra of the preheated samples showed no evidence of decomposition. As noted above, **1** and **2** were previously reported to undergo thermal decomposition starting at about 150 °C in the thermogravimetric analyses [64]. The solid state decomposition temperatures reported herein for **1** and **2** are much higher. Complexes **7** and **8** showed extensive decomposition in the ^{1}H NMR spectra after the melting point experiments. In terms of thermal stability trends, the hafnium complexes **4**–**6** have decomposition temperatures that are 20–25 °C higher than the zirconium analogs **1**–**3**. The complexes derived from the N-isopropylisobutyramide ligand exhibit the highest solid state decomposition temperatures (**2**, 335; **5**, 360 °C). In previous ALD studies, we have found that the solid state decomposition temperatures of metal-containing precursors are often very similar to the upper temperature limit of self-limited ALD growth [66–69]. Accordingly, several of the precursors described herein may exhibit self-limited ALD growth at >300 °C. Such high growth temperatures should favor the desirable tetragonal and cubic phases of ZrO_2 and HfO_2.

In preparative sublimation studies, 0.5–1.0 g of previously sublimed samples of **1**–**6** were resublimed between 130 and 140 °C at 0.05 Torr, and the sublimed recoveries and nonvolatile residues were determined. Complete sublimation of the samples was achieved within 4–6 h by conducting the experiments at temperatures ~20 °C higher than the sublimation temperatures reported in the experimental section. Complexes **7** and **8** were not studied, since they undergo extensive decomposition under sublimation conditions. The recoveries of sublimed **1**–**6** ranged between 84.5 and 96.4%, and showed no obvious trend with structure (Table 4). The air sensitivity of **1**–**6** complicated efforts to obtain higher recovered yields, and losses of up to 10% could have occurred upon isolation, depending upon the morphologies of the solids and their

Please cite this article in press as: M.C. Karunarathne, et al., Journal of Organometallic Chemistry (2017), http://dx.doi.org/10.1016/j.jorganchem.2017.03.003

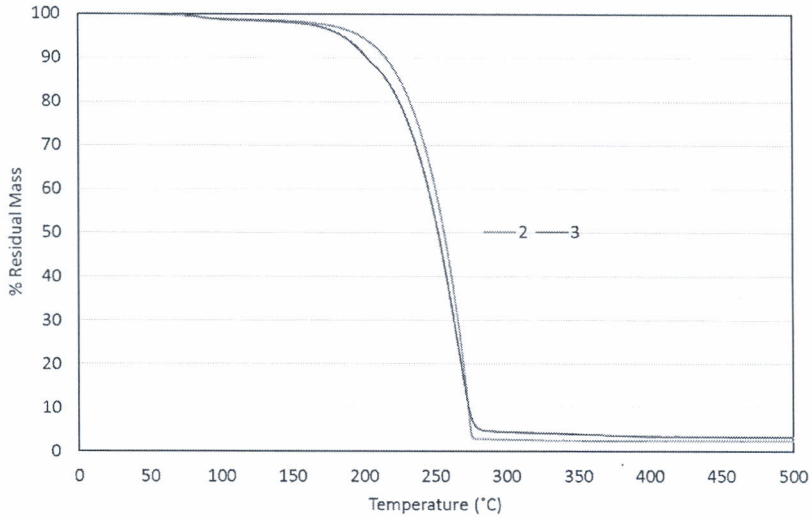

Fig. 6. Thermogravimetric analyses of **2** and **3**.

Table 4
Preparative sublimation data and decomposition temperatures for **1–8**.

Compound	Preparative sublimation temperature (°C/0.05 Torr)	% Recovery	% Nonvolatile residue	Decomposition temperature (°C)
1	135	92.2	3.06	280
2	130	84.5	1.42	335
3	130	96.4	0.95	270
4	140	94.9	1.09	300
5	135	86.8	1.31	360
6	130	95.8	0.68	290
7	130	<5%	–	218
8	130	<5%	–	263

sensitivities to static electricity buildup in the glove box. However, nonvolatile residues for **1–6** were ≤3%, indicating a minimum amount of decomposition during sublimation. Precursors **1–6** exhibit moderate sublimation temperatures with high recoveries and low nonvolatile residues, which indicate that they may be good CVD and ALD precursors. For comparison, $Hf(iPrOC(O)NiPr)_4$ and $Hf(MeEtNC(O)NiPr)_4$ were evaluated as CVD precursors for the growth of HfO_2 films [51]. $Hf(MeEtNC(O)NiPr)_4$ showed a narrow temperature window between sublimation and thermal decomposition, and was thus not explored further as a precursor. $Hf(i-PrOC(O)NiPr)_4$ could be vaporized at 80 °C over > 3 h, but showed a complicated thermogravimetric trace that likely entails decomposition at ca. 150–200 °C [51]. It is possible that the decompositions of $Hf(iPrOC(O)NiPr)_4$ and $Hf(MeEtNC(O)NiPr)_4$ occur by deinsertion of iPrN=C=O at moderate temperatures. In the present work, **1–8** are much more stable thermally than $Hf(iPrOC(O)NiPr)_4$ and $Hf(MeEtNC(O)NiPr)_4$, because low energy decomposition paths are eliminated and isocyanate deinsertion is disfavored by the alkyl substituents on the amidate ligand core carbon atoms. $Zr(iPrC(O)NiPr)_4$ was explored as a single-source precursor to ZrO_2 films using aerosol-assisted CVD between 350 and 600 °C [64]. These depositions afforded cubic ZrO_2 films, consistent with the high growth temperatures.

3. Conclusions

This work describes the synthesis, structure, and characterization of the zirconium(IV) and hafnium(IV) complexes **1–8** that contain κ^2-N,O-amidate ligands as the anionic donors. These complexes are monomeric and adopt approximate dodecahedral geometry in the solid state. Complexes **1–6**, which contain larger alkyl groups on the amidate core nitrogen and carbon atoms, are thermally robust and can be isolated in moderate to good yields upon direct sublimation from the crude reaction mixtures. By contrast, **7** and **8** contain smaller alkyl groups on the amidate core nitrogen and carbon atoms (**7**) or a hydrogen atom on the amidate core carbon atom (**8**), and undergo extensive decomposition upon attempted sublimation. Accordingly, bulky alkyl groups appear to be required for high thermal stability, most likely because they reduce intermolecular interactions. The thermal stability and volatility of **1–8** were evaluated. Complexes **2** and **3** undergo single step sublimations in thermogravimetric analyses, and have low nonvolatile residues. Complexes **1–6** undergo sublimation on a preparative scale from 130 to 140 °C at 0.05 Torr, with 84.5–95.8% sublimed recoveries and 0.68–3.06% nonvolatile residues. Solid state decomposition temperatures for the zirconium complexes **1–3** range between 270 and 335 °C and 290–360 °C for the hafnium complexes **4–6**. Complexes **2**, **4**, and **5** have thermal decomposition temperatures of >300 °C and sublime at moderate temperatures. These compounds therefore have useful properties for application as chemical vapor deposition and atomic layer deposition precursors.

4. Experimental section

4.1. General considerations

All manipulations were performed under argon using standard

Please cite this article in press as: M.C. Karunarathne, et al., Journal of Organometallic Chemistry (2017), http://dx.doi.org/10.1016/j.jorganchem.2017.03.003

glovebox and Schlenk line techniques. Toluene was freshly distilled from sodium, tetrahydrofuran was distilled from a purple solution of sodium benzophenone ketyl, and hexane was distilled from phosphorus pentoxide. N-*tert*-butylformamide and tetrakis(dimethyl)amidozirconium were purchased from Sigma-Aldrich. Tetrakis(dimethyl)amidohafnium was purchased from Strem Chemicals, Inc. *N*-methylacetamide was purchased from Oakwood Chemicals. Commercial chemicals were used as received. N-*tert*-butylacetamide [70], N-isopropylisobutyramide [71], and N-isopropylacetamide [72] were prepared and purified by reported methods.

^{1}H and ^{13}C{^{1}H} NMR spectra were obtained at 500 and 125 MHz in benzene-d_6. Infrared spectra were obtained using Nujol as the medium. Elemental analyses were performed by Midwest Microlab, Indianapolis, Indiana. Melting points and solid state decomposition temperatures were obtained on a Haake-Buchler HBI digital melting point apparatus and are uncorrected. Thermogravimetric analyses of **2** and **3** were carried out with a Mettler-Toledo TGA/DSC 1 instrument situated in a nitrogen filled glove box. The heating rate was 10 °C/min. Vapor pressure measurements of **2** and **3** were estimated using the Knudsen effusion method [73,74]. The latter two sets of measurements were carried out at Nova-Kem, LLC.

4.2. Compound preparation

4.2.1. Preparation of Zr(MeC(O)NtBu)$_4$ **1**

A 100 mL Schlenk flask fitted with a reflux condenser was charged with tetrakis(dimethylamido)zirconium (0.200 g, 0.748 mmol) and N-*tert*-butylacetamide (0.344 g, 2.99 mmol). With vigorous stirring, 20 mL of toluene was added and the colorless reaction mixture was then refluxed for 3 h. Upon cooling to room temperature, the volatile components were removed under reduced pressure to give a white solid. Sublimation of the crude solid at 120 °C/0.05 Torr afforded **1** as colorless crystals (0.332 g, 81%): mp 255–258 °C; IR (Nujol, cm^{-1}) 1563 (s), 1365 (s), 1339 (s), 1217 (s), 1050 (m), 1036 (m), 994 (m), 922 (w), 838 (m), 778 (m), 602 (s), 583 (s); ^{1}H NMR (C_6D_6, 23 °C, δ) 1.89 (s, 12H, CH_3), 1.34 (s, 36H, C(CH_3)$_3$); ^{13}C{^{1}H} NMR (C_6D_6, 23 °C, ppm) 182.09 (s, *C*=O), 52.26 (s, C(CH_3)$_3$), 31.23 (s, C(CH_3)$_3$), 22.26 (s, CH_3).

Anal. Calcd for $C_{24}H_{48}N_4O_4Zr$: C, 52.61; H, 8.83; N, 10.23. Found: C, 52.55; H, 8.94; N, 10.27.

4.2.2. Preparation of Zr(iPrC(O)NiPr)$_4$ **2**

In a fashion similar to the preparation of **1**, treatment of tetrakis(dimethylamido)zirconium (0.200 g, 0.748 mmol) with N-isopropylisobutyramide (0.386 g, 2.99 mmol) in refluxing toluene (20 mL) for 3 h afforded **2** as a colorless crystalline solid (0.393 g, 87%) upon sublimation at 115 °C/0.05 Torr: mp 285–288 °C; IR (Nujol, cm^{-1}) 1563 (s), 1416 (s), 1364 (s), 1347 (s), 1312 (s), 1178 (s), 1127 (m), 1078 (s), 1021 (s), 927 (w), 900 (m), 875 (m), 758 (m), 645 (m), 580 (s); ^{1}H NMR (C_6D_6, 23 °C, δ) 3.56 (septet, J = 6.5 Hz, 4H, CH(CH$_3$)$_2$), 2.59 (septet, J = 7.0 Hz, 4H, CH(CH$_3$)$_2$), 1.32 (d, J = 6.5 Hz, 24H, NCH(*C*H$_3$)$_2$), 1.12 (d, J = 7.0 Hz, 24H, CCH(*C*H$_3$)$_2$); ^{13}C{^{1}H} NMR (C_6D_6, 23 °C, ppm) 188.30 (s, *C*=O), 47.73 (s, NCH(CH$_3$)$_2$), 28.65 (s, CCH(CH$_3$)$_2$), 24.58 (s, NCH(*C*H$_3$)$_2$), 19.34 (s, CCH(*C*H$_3$)$_2$).

Anal. Calcd for $C_{28}H_{56}N_4O_4Zr$: C, 55.68; H, 9.35; N, 9.28. Found: C, 55.52; H, 9.28; N, 9.34.

4.2.3. Preparation of Zr(MeC(O)NiPr)$_4$ **3**

A 100 mL Schlenk flask fitted with a reflux condenser was charged with tetrakis(dimethylamido)zirconium (0.200 g, 0.748 mmol) and toluene (10 mL). A solution of N-isopropylacetamide (0.302 g, 2.99 mmol) in toluene (10 mL) was added slowly and the resultant mixture was refluxed for 3 h. Upon cooling to room temperature, the volatile components were removed under reduced pressure and sublimation of the crude solid at 110 °C/0.05 Torr afforded **3** as colorless crystals (0.188 g, 51%): mp 206–209 °C; IR (Nujol, cm^{-1}) 1576 (s), 1456 (s), 1403 (s), 1363 (s), 1342 (s), 1319 (m), 1186 (s), 1170 (m), 1126 (m), 1051 (m), 987 (m), 886 (m), 822 (m), 814 (m), 614 (s), 582 (s); ^{1}H NMR (C_6D_6, 23 °C, δ) 3.34 (septet, J = 6.2 Hz, 4H, CH(CH$_3$)$_2$), 1.71 (s, 12H, CH_3), 1.24 (d, J = 6.2 Hz, 24H, CH(*C*H$_3$)$_2$); ^{13}C{^{1}H} NMR (C_6D_6, 23 °C, ppm) 183.00 (s, *C*=O), 48.94 (s, *C*H(CH$_3$)$_2$), 23.86 (s, CH(*C*H$_3$)$_2$), 17.06 (s, *C*H$_3$).

Anal. Calcd for $C_{20}H_{40}N_4O_4Zr$: C, 48.85; H, 8.20; N, 11.39. Found: C, 48.69; H, 8.06; N, 11.44.

4.2.4. Preparation of Hf(MeC(O)NtBu)$_4$ **4**

In a fashion similar to the preparation of **1**, treatment of tetrakis(dimethylamido)hafnium (0.200 g, 0.563 mmol) with N-*tert*-butylacetamide (0.260 g, 2.25 mmol) in refluxing toluene (15 mL) for 3 h afforded **4** as a colorless crystalline solid (0.297 g, 83%) upon sublimation at 125 °C/0.05 Torr: mp 255–258 °C; IR (Nujol, cm^{-1}) 1562 (s), 1389 (s), 1364 (s), 1341 (s), 1218 (s), 1053 (m), 1036 (m), 995 (m), 922 (w), 839 (m), 799 (w), 779 (m), 754 (w), 604 (m), 588 (m); ^{1}H NMR (C_6D_6, 23 °C, δ) 1.89 (s, 12H, CH_3), 1.34 (s, 36H, C(CH_3)$_3$); ^{13}C{^{1}H} NMR (C_6D_6, 23 °C, ppm) 181.68 (s, *C*=O), 51.97 (s, *C*(CH$_3$)$_3$), 31.34 (s, C(*C*H$_3$)$_3$), 22.76 (s, CH_3).

Anal. Calcd for $C_{24}H_{48}HfN_4O_4$: C, 45.38; H, 7.62; N, 8.82. Found: C, 45.22; H, 7.96; N, 8.91.

4.2.5. Preparation of Hf(iPrC(O)NiPr)$_4$ **5**

In a fashion similar to the preparation of **1**, treatment of tetrakis(dimethylamido)hafnium (0.200 g, 0.563 mmol) with N-isopropylisobutyramide (0.291 g, 2.25 mmol) in refluxing toluene (15 mL) for 3 h afforded **5** as a colorless crystalline solid (0.308 g, 79%) upon sublimation at 115 °C/0.05 Torr: mp 283–286 °C; IR (Nujol, cm^{-1}) 1565 (s), 1421 (s), 1365 (s), 1350 (s), 1313 (s), 1261 (m), 1180 (s), 1127 (m), 1079 (s), 1023 (s), 927 (w), 900 (m), 876 (m), 798 (w), 759 (m), 647 (m), 581 (s); ^{1}H NMR (C_6D_6, 23 °C, δ) 3.68 (septet, J = 6.5 Hz, 4H, CH(CH$_3$)$_2$), 2.57 (septet, J = 7.0 Hz, 4H, CH(CH$_3$)$_2$), 1.31 (d, J = 6.5 Hz, 24H, NCH(*C*H$_3$)$_2$), 1.13 (d, J = 7.0 Hz, 24H, CCH(*C*H$_3$)$_2$); ^{13}C{^{1}H} NMR (C_6D_6, 23 °C, ppm) 187.80 (s, *C*=O), 47.39 (s, NCH(CH$_3$)$_2$), 29.10 (s, CCH(CH$_3$)$_2$), 24.59 (s, NCH(*C*H$_3$)$_2$), 19.33 (s, CCH(*C*H$_3$)$_2$).

Anal. Calcd for $C_{28}H_{56}HfN_4O_4$: C, 48.65; H, 8.17; N, 8.11. Found: C, 48.76; H, 8.14; N, 8.18.

4.2.6. Preparation of Hf(MeC(O)NiPr)$_4$ **6**

In a fashion similar to the preparation of **1**, treatment of tetrakis(dimethylamido)hafnium (0.200 g, 0.563 mmol) with N-isopropylacetamide (0.228 g, 2.25 mmol) in refluxing toluene (15 mL) for 3 h afforded **6** as colorless crystals (0.219 g, 67%) upon sublimation at 105 °C/0.05 Torr: mp 207–210 °C; IR (Nujol, cm^{-1}) 1579 (s), 1404 (s), 1365 (s), 1344 (s), 1319 (m), 1188 (s), 1170 (m), 1127 (m), 1053 (m), 988 (m), 887 (m), 823 (m), 816 (m), 618 (s), 584 (s); ^{1}H NMR (C_6D_6, 23 °C, δ) 3.47 (septet, J = 6.5 Hz, 4H, CH(CH$_3$)$_2$), 1.70 (s, 12H, CH_3), 1.23 (d, J = 6.5 Hz, 24H, CH(*C*H$_3$)$_2$); ^{13}C{^{1}H} NMR (C_6D_6, 23 °C, ppm) 182.44 (s, *C*=O), 48.67 (s, *C*H(CH$_3$)$_2$), 23.86 (s, CH(*C*H$_3$)$_2$), 17.37 (s, CH_3).

Anal. Calcd for $C_{20}H_{40}HfN_4O_4$: C, 41.48; H, 6.96; N, 9.68. Found: C, 41.32; H, 6.85; N, 9.77.

4.2.7. Preparation of Zr(MeC(O)NMe)$_4$ **7**

Two 100 mL Schlenk flasks were charged separately with tetrakis(dimethylamido)zirconium (0.250 g, 0.934 mmol) and *N*-methylacetamide (0.273 g, 3.74 mmol). To each flask was added toluene (10 mL). The flask containing the zirconium solution was cooled to −78 °C using a dry ice/acetone bath. The ligand solution was transferred into the zirconium flask via cannula to generate a

Please cite this article in press as: M.C. Karunarathne, et al., Journal of Organometallic Chemistry (2017), http://dx.doi.org/10.1016/j.jorganchem.2017.03.003

clear, colorless solution. Upon warming to room temperature, the reaction flask was fitted with a reflux condenser and the solution was then refluxed for 1 h. Upon cooling to room temperature, the volatile components were removed under reduced pressure from the turbid yellow solution to yield an off-white solid. The white solid was extracted with hexane (20 mL), and then the hexane solution was filtered through a 2-cm pad of Celite on a coarse glass frit to afford a colorless solution. Removal of the volatile components under reduced pressure afforded **7** as an off-white powder (0.275 g, 77% crude yield). Sublimation of crude material at 100 °C/0.05 Torr afforded **7** as colorless crystals (0.018 g, 5%): mp 180–181 °C; IR (Nujol, cm^{-1}) 1633 (s), 1583 (s), 1344 (s), 1282 (m), 1155 (m), 993 (m), 912 (s), 848 (s), 825 (s), 721 (s), 669 (s), 638 (s), 584 (s); ^1H NMR (C_6D_6, 23 °C, δ) 2.83 (s, 12H, NCH_3), 1.64 (s, 12H, CCH_3); $^{13}C\{^1H\}$ NMR (C_6D_6, 23 °C, ppm) 168.42 (s, *C*=O), 33.10 (s, NCH_3), 17.45 (s, CCH_3). A CHN microanalysis was not conducted because of the low isolated yield of **7**.

*4.2.8. Preparation of $Zr(HC(O)NtBu)_4$ **8***

In a fashion similar to **7**, treatment of tetrakis(dimethylamido) zirconium (0.250 g, 0.934 mmol) with *N-tert*-butylformamide (0.378 g, 3.74 mmol) afforded crude **8** as a fine, off-white powder (0.210 g, 46%). Sublimation of the crude material at 120 °C/0.05 Torr afforded **8** as colorless crystals (0.005 g, 1%): mp 243–244 °C; IR (Nujol, cm^{-1}) 1584 (s), 1560 (s), 1344 (s), 1280 (m), 1238 (s), 1211 (s), 999 (s), 806 (s), 721 (s), 669 (s); ^1H NMR (C_6D_6, 23 °C, δ) 8.65 (s, 4H, *CH*), 1.22 (s, 36H, $C(CH_3)_3$); $^{13}C\{^1H\}$ NMR (C_6D_6, 23 °C, ppm) 174.75 (s, *C*=O), 53.79 (s, $C(CH_3)_3$), 31.02 (s, $C(CH_3)_3$). A CHN microanalysis was not conducted because of the low isolated yield of **8**.

4.2.9. X-ray diffraction studies

CCDC-1530353 (**1**), CCDC-1530354 (**3**), CCDC-1530355 (**6**), CCDC-1530356 (**7**), and CCDC-1530357 (**8**) contain the supplementary crystallographic data for this paper. The data can be obtained free of charge from the Cambridge Crystallographic Data Centre, 12 Union Road, Cambridge, CB2 1EZ, UK (fax: ++44-1223-336-033; email: deposit@ccdc.cam.ac.uk). Diffraction data were measured on a Bruker X8 APEX-II kappa geometry diffractometer with Mo radiation and a graphite monochromator. Frames were collected at 100 K as a series of sweeps with the detector at 40 mm and 0.3–0.5° between each frame. For **1**, **3**, and **6**, APEX-II [75] and SHELX-97 [76] software was used in the collection and refinement of the models. For **7** and **8**, the frames were integrated with the Bruker SAINT software package using a narrow-frame algorithm with Olex2 [77], the structure was solved with the ShelXT [78] structure solution program using direct methods, and was refined with the ShelXL [79] refinement package using least squares minimization.

Acknowledgments

We are grateful to the U.S. National Science Foundation (grant nos. CHE-0910475 and CHE-1607973) for generous support of this research. We thank Drs. Marek P. Boleslawski and Andrey V. Korolev of Nova-Kem, LLC, Germantown, Wisconsin for conducting the thermogravimetric analyses and the vapor pressure measurements.

Appendix A. Supplementary data

Supplementary data related to this article can be found at http://dx.doi.org/10.1016/j.jorganchem.2017.03.003.

References

[1] M.T. Bohr, R.S. Chau, T. Ghani, K. Mistry, IEEE Spectr. 44 (2007) 29–35.
[2] K. Derbyshire, Solid State Technol. 51 (2008) 24–29.
[3] G.D. Wilk, R.M. Wallace, Appl. Phys. Lett. 74 (1999) 2854–2856.
[4] W. He, D.S.H. Chan, S.J. Kim, Y.S. Kim, S.T. Kim, B.J. Cho, J. Electrochem. Soc. 155 (2008) G189–G193.
[5] G. Seguini, S. Spiga, E. Bonera, M. Fanciulli, A.R. Huamantinco, C.J. Först, C.R. Ashman, P.E. Blochl, A. Dimoulas, G. Mavrou, Appl. Phys. Lett. 88 (2006) 202903.
[6] Y. Yamamoto, K. Kita, K. Kyuno, A. Toriumi, Appl. Phys. Lett. 89 (2006) 032903.
[7] Y.F. Loo, S. Taylor, R.T. Murray, A.C. Jones, P.R. Chalker, J. Appl. Phys. 99 (2006) 103704.
[8] W.S. Kim, S.K. Park, D.Y. Moon, B.W. Kang, H.D. Kim, J.W. Park, Thin Solid Films 517 (2009) 3900–3903.
[9] I. Ferain, L. Pantisano, A. Kottantharayil, J. Petry, L. Trojman, N. Collaert, M. Jurczak, K.D. Meyer, Microelectron. Eng. 84 (2007) 1882–1885.
[10] B. Xia, M.L. Fisher, H. Stemper, A. Misra, Thin Solid Films 516 (2008) 5460–5464.
[11] H. Kim, K.C. Saraswat, P.C. McIntyre, J. Mater. Res. 20 (2005) 3125–3132.
[12] S.J. Yun, J.B. Koo, J.W. Lim, S.H. Kim, Electrochem. Solid-State Lett. 10 (2007) H90–H93.
[13] H. Ishii, A. Nakajima, S. Yokoyama, J. Appl. Phys. 95 (2004) 536–542.
[14] I. Kim, J. Koo, J. Lee, H. Jeon, Jpn. J. Appl. Phys. 45 (2006) 919–925.
[15] R.C. Smith, N. Hoilien, C.J. Taylor, T. Ma, S.A. Campbell, J.T. Roberts, M. Copel, D.A. Buchanan, M. Gribelyuk, W.L. Gladfelter, J. Electrochem. Soc. 147 (2000) 3472–3476.
[16] S. Bang, S. Lee, S. Jeon, S. Kwon, W. Jeong, S. Kim, H. Jeon, J. Electrochem. Soc. 155 (2008) H633–H637.
[17] R.I. Hegde, D.H. Triyoso, S.B. Samavedam, B.E. White Jr., J. Appl. Phys. 101 (2007) 074113.
[18] B.S. Sahu, S.V.N. Pammi, N.-J. Seong, S.-G. Yoon, J. Vac. Sci. Technol. B 26 (2008) 1338–1343.
[19] Z.M. Rittersma, E. Naburgh, T. Dao, A.H.C. Hendriks, W.F.A. Besling, E. Tois, E.V. Vainonen-Ahlgren, M. Tuominen, S. Haukka, Electrochem. Solid-State Lett. 6 (2003) F21–F23.
[20] J. Kim, K. Yong, Electrochem. Solid-State Lett. 7 (2004) F35–F37.
[21] L. Kang, B.H. Lee, W.-J. Qi, Y. Jeon, R. Nieh, S. Gopalan, K. Onishi, J.C. Lee, IEEE Electron Device Lett. 21 (2000) 181–183.
[22] R. Mantovan, M. Georgieva, M. Perego, H.L. Lu, S. Cocco, A. Zenkevich, G. Scarel, M. Fanciulli, Acta Phys. Pol. A 112 (2007) 1271–1280.
[23] S. Maikap, H.Y. Lee, T.-Y. Wang, P.-J. Tzeng, C.C. Wang, L.S. Lee, K.C. Liu, J.-R. Yang, M.-J. Tsai, Semicond. Sci. Technol. 22 (2007) 884–889.
[24] H.-Y. Lee, P.-S. Chen, C.-C. Wang, S. Maikap, P.-J. Tzeng, C.-H. Lin, L.-S. Lee, M.-J. Tsai, Jpn. J. Appl. Phys. 46 (2007) 2175–2179.
[25] E.E. Hoppe, R.S. Sorbello, C.R. Aita, J. Appl. Phys. 101 (2007) 123534.
[26] V. Fomenko, E.P. Gusev, E. Borguet, J. Appl. Phys. 97 (2005) 083711.
[27] G. He, Q. Fang, J.X. Zhang, L.Q. Zhu, M. Liu, L.D. Zhang, Nanotechnology 16 (2005) 1641–1647.
[28] M. Leskelä, M. Ritala, Angew. Chem. Int. Ed. 42 (2003) 5548–5554.
[29] S.M. George, Chem. Rev. 110 (2010) 111–131.
[30] M. Putkonen, L. Niinistö, Top. Organomet. Chem. 9 (2005) 125–145.
[31] C. Thelander, L.E. Fröberg, C. Rehnstedt, L. Samuelson, L.-E. Wernersson, IEEE Electron Dev. Lett. 29 (2008) 206–208.
[32] T. Blanquart, J. Niinistö, M. Ritala, M. Leskelä, Chem. Vap. Depos. 20 (2014) 189–208.
[33] J. Niinistö, K. Kukli, M. Keikkilä, M. Ritala, M. Leskelä, Adv. Eng. Mater 11 (2009) 223–234.
[34] A.C. Jones, H.C. Aspinall, P.R. Chalker, R.J. Potter, K. Kukli, A. Rahtu, M. Ritala, M. Leskelä, J. Mater. Chem. 14 (2004) 3101–3112.
[35] K. Kukli, M. Kemell, J. Köykkä, K. Mizohata, M. Vehkamäki, M. Ritala, M. Leskelä, Thin Solid Films 589 (2015) 597–604.
[36] K. Kukli, M. Ritala, T. Sajavaara, J. Keinonen, M. Leskelä, Thin Solid Films 416 (2002) 72–79.
[37] S.K. Kim, C.S. Hwang, Electrochem. Solid St. Lett. 11 (2008) G9–G11.
[38] K. Kukli, M. Ritala, J. Lu, A. Harsta, M. Leskelä, J. Electrochem. Soc. 151 (2004) F189–F193.
[39] D.M. Hausmann, E. Kim, J. Becker, R.G. Gordon, Chem. Mater 14 (2002) 4350–4358.
[40] S. Wada, A. Sakurai, N. Yamada, T. Watanabe, H. Uchiuzo, ECS Trans. 25 (2009) 209–216.
[41] R. Matero, M. Ritala, M. Leskelä, T. Sajavaara, A.C. Jones, J.L. Roberts, Chem. Mater 16 (2004) 5630–5636.
[42] K. Kukli, M. Ritala, M. Leskelä, T. Sajavaara, J. Keinonen, A.C. Jones, J.L. Roberts, Chem. Vap. Depos. 9 (2003) 315–320.
[43] J.-S. Jung, S.-K. Lee, C.-S. Hong, J.-H. Shin, J.-M. Kim, J.-G. Kang, Thin Solid Films 589 (2015) 831–837.
[44] J. Niinistö, T. Hatanpää, M. Kariniemi, M. Mäntymäki, L. Costelle, K. Mizohata, K. Kukli, M. Ritala, M. Leskelä, Chem. Mater 24 (2012) 2002–2008.
[45] J. Niinistö, M. Mäntymäki, K. Kukli, L. Costelle, E. Puukilainen, M. Ritala, M. Leskelä, J. Cryst. Growth 312 (2010) 245–249.
[46] S. Dueñas, H. Castán, H. García, A. Gómez, L. Bailón, K. Kukli, J. Niinistö, M. Ritala, M. Leskelä, Microelectron. Eng. 86 (2009) 1689–1691.
[47] J. Niinistö, K. Kukli, M. Kariniemi, M. Ritala, M. Leskelä, N. Blasco, A. Pinchart, C. Lachaud, N. Laaroussi, Z. Wang, C. Dussarrat, J. Mater. Chem. 18 (2008) 5243–5247.
[48] M. Kaipio, T. Blanquart, M. Banerjee, K. Xu, J. Niinistö, V. Longo, K. Mizohata, A. Devi, M. Ritala, M. Leskelä, Chem. Vap. Depos. 20 (2014) 209–216.

Please cite this article in press as: M.C. Karunarathne, et al., Journal of Organometallic Chemistry (2017), http://dx.doi.org/10.1016/j.jorganchem.2017.03.003

[49] T. Blanquart, J. Niinistö, N. Aslam, M. Banerjee, Y. Tomczak, M. Gavagnin, V. Longo, E. Puukilainen, H.D. Wanzenboeck, W.M.M. Kessels, A. Devi, S. Hoffman-Eifert, M. Ritala, M. Leskelä, Chem. Mater 25 (2013) 3088–3095.
[50] J. Niinistö, M. Putkonen, L. Niinistö, F. Song, P. Williams, P.N. Heys, R. Odedra, Chem. Mater 19 (2007) 3319–3324.
[51] R. Pothiraja, A.P. Milanov, D. Barreca, A. Gasparotto, H.-W. Becker, M. Winter, R.A. Fischer, A. Devi, Chem. Commun. (2009) 1978–1980.
[52] H.H. Gibbs, C.V. Breder, Adv. Chem. 142 (1975) 442–457.
[53] P.R. Payne, R.K. Thompson, D.M. Medeiros, G. Wan, L.L. Schafer, Dalton Trans. 42 (2013) 15670–15677.
[54] J.M.P. Lauzon, L.L. Schafer, Z. Anorg, Allg. Chem. 641 (2015) 128–135.
[55] N. Yonson, J.C.-H. Yim, L.L. Schafer, Inorg. Chim. Acta 422 (2014) 14–20.
[56] R.O. Ayinla, T. Gibson, L.L. Schafer, J. Organomet. Chem. 696 (2011) 50–60.
[57] G. Zi, F. Zhang, L. Xiang, Y. Chen, W. Fang, H. Song, Dalton Trans. 39 (2010) 4048–4061.
[58] G. Zi, X. Liu, L. Xiang, H. Song, Organometallics 28 (2009) 1127–1137.
[59] M.C. Wood, D.C. Leitch, C.S. Yeung, J.A. Kozak, L.L. Schafer, Angew. Chem. Int. Ed. 46 (2007) 354–358.
[60] A.V. Lee, L.L. Schafer, Eur. J. Inorg. Chem. (2007) 2243–2255.
[61] R.K. Thompson, J.A. Bexrud, L.L. Schafer, Organometallics 25 (2006) 4069–4071.
[62] R.K. Thompson, F.E. Zahariev, Z. Zhang, B.O. Patrick, Y.A. Wang, L.L. Schafer, Inorg. Chem. 44 (2005) 8680–8689.
[63] R.K. Thompson, B.O. Patrick, L.L. Schafer, Can. J. Chem. 83 (2005) 1037–1042.
[64] A.L. Catherall, M.S. Hill, A.L. Johnson, G. Kociok-Kohn, M.F. Mahon, J. Mater. Chem. C 4 (2016) 10731–10739.
[65] N.N. Greenwood, A. Earnshaw, Chemistry of the Elements, second ed., Butterworth-Heinemann, Oxford, 1997, p. 957.
[66] T.J. Knisley, T.C. Ariyasena, T. Sajavaara, M.J. Saly, C.H. Winter, Chem. Mater 23 (2011) 4417–4419.
[67] M.K. Wiedmann, M.C. Karunarathne, R.J. Baird, C.H. Winter, Chem. Mater 22 (2010) 4400–4405.
[68] M.J. Saly, M.J. Heeg, C.H. Winter, Inorg. Chem. 48 (2009) 5303–5312.
[69] J.P. Klesko, M.M. Kerrigan, C.H. Winter, Chem. Mater 28 (2016) 700–703.
[70] A.C. Cope, N.A. LeBel, H.-H. Lee, W.R. Moore, J. Am. Chem. Soc. 79 (1957) 4720–4729.
[71] N. De Kimpe, R. Verhe, L. De Buyck, J. Chys, N. Schamp, Org. Prep. Proced. Int. 10 (1978) 149–156.
[72] H.E. Johnson, D.G. Crosby, J. Org. Chem. 27 (1962) 2205–2206.
[73] M.G. Rossman, J. Yarwood, J. Chem. Phys. 21 (1953) 1406–1407.
[74] T.H. Swan, E. Mack Jr., J. Am. Chem. Soc. 47 (1925) 2112–2116.
[75] APEX II Collection and Processing Programs are distributed by the Manufacturer, Bruker AXS Inc., Madison, WI, USA, 2009.
[76] G.M. Sheldrick, Acta Crystallogr. A 64 (2008) 112–122.
[77] O.V. Dolomanov, L.J. Bourhis, R.J. Gildea, J.A.K. Howard, H. Puschmann, J. Appl. Cryst. 42 (2009) 339–341.
[78] G.M. Sheldrick, Acta Cryst. A71 (2015) 3–8.
[79] G.M. Sheldrick, Acta Cryst. C71 (2015) 3–8.

Please cite this article in press as: M.C. Karunarathne, et al., Journal of Organometallic Chemistry (2017), http://dx.doi.org/10.1016/j.jorganchem.2017.03.003